Supporting Information

Synergistic effect of surface metal vacancies and Schottky junction on high-transconductance organic photoelectrochemical transistor aptasensing

Jingjie Lai,[a] Cunhao Fan,[a] Fuheng You,[b] Yuanhao Liu,[a] Xilong Zhou,[a] Yuhang Lin,[a] Lijun Ding[b] and Kun Wang*[a]*

[a]*School of Chemistry and Chemical Engineering, Jiangsu University, Zhenjiang 212013, PR China. E-mail: wangkun@ujs.edu.cn (K. Wang)*

[b]*Key Laboratory for Theory and Technology of Intelligent Agricultural Machinery and Equipment, Jiangsu University, Zhenjiang 212013, PR China. E-mail: ljding@ujs.edu.cn (L.J. Ding)*

Content

1. Materials and Apparatus

1.1 Experimental materials

Zinc acetate ($Zn(Ac)_2$, AR) and (3,4-ethylenedioxythiophene): poly (styrene sulfonic acid) (PEDOT: PSS) were purchased from Shanghai Macklin Biochemical Co., Ltd. Methenamine ($C_6H_{12}N_4$, AR), Zinc nitrate ($Zn(NO_3)_2 \cdot 6H_2O$, AR), Choline chloride ($C_5H_{14}ClNO$, AR), Ethylene glycol ($C_2H_6O_2$), Palladium nitrate ($Pd(NO_3)_2$), Borane ammonia complex ($NH_3 \cdot BH_3$), Dimethyl sulfoxide (DMSO), Sodium dihydrogen phosphate (NaH_2PO_4, AR), Dibasic sodium phosphate (Na_2HPO_4, AR), Chitosan (CHI, AR, 99.0%), Glutaraldehyde (GA, AR) and Bovine serum albumin (BSA, AR) were purchased from Sinopharm Chemical Reagent Co., Ltd. (China). Ochratoxin A (OTA), aflatoxin B1 (AFB1) were purchased from Sigma-Aldrich (USA). Other interferents including ochratoxin B (OTB), ochratoxin C (OTC) and T-2 toxin were purchased from Puhuashi Technology Company, Beijing. Phosphate-buffered saline (PBS) of different pH were prepared by mixing 0.1 mol/L stock solutions of NaH_2PO_4 and Na_2HPO_4 at specific ratios, and the washing buffer was prepared by 0.01 mol/L PBS (pH 7.4). Ultrapure water was used throughout the experiment.

OTA aptamer was purchased from Sangon Biological Engineering Technology & Services Co. Ltd, Shanghai, and the sequences as follows:[1] 5'-NH_2-GAT CGG GTG TGG GTG GCG TAA AGG GAG CAT CGG ACA-3'.

1.2 Apparatus

The morphologies of nanomaterials were observed by scanning electron microscopy (SEM, JSM-7800F, Japan) and transmission electron microscopy (TEM, JEOL JEM-AFM, Japan). X-ray diffractometer equipped with (Bruker, Germany) high-intensity Cu Kα (λ = 1.5406) radiation was used to record the X-ray diffraction (XRD) pattern. The absorption spectrum was tested by UV-vis spectrophotometer (UV2550, Shimadzu, Japan) from 200 to 1000 nm with $BaSO_4$ as reflectance sample. X-ray photoelectron spectroscopy (XPS) measurements were measured on Thermo Scientific K-Alpha X-ray photoelectron spectrometer with Al Kα X-rays as the excitation source. Electron paramagnetic resonance (EPR) spectra were recorded at room temperature on

an EPR spectrometer (Bruker EMX PLUS). The photoelectrochemical (PEC), electrochemical impedance spectroscopy (EIS), and cyclic voltammograms (CV), Mott-Schottky measurements were performed using a conventional three-electrode system (CHI 660E, Chen Hua Instruments Co., Ltd. Shanghai, China). The OPECT measurements were monitored by a multichannel potentiostat (CHI 1010C, Chen Hua Instruments Co., Ltd. Shanghai, China). All of the electrochemical measurements used Xe lamp (PLS-SXE 300C (BF) Beijing perfect Light Technology Co., Ltd.) as the light irradiation source for the whole detection.

2. Experimental Section

2.1 Integrated flexible electrode design

First, the ITO-PET flexible substrate was cut into uniform slices with the size of 10 mm×13 mm. According to the designed drawing (Fig. S1A), gate electrode, source and drain electrodes were etched onto the slice surface using laser etching technology. The obtained integrated flexible electrodes were ultrasonically cleaned with toluene, acetone, ethanol and deionized water respectively, and then dried by nitrogen for later use. Fig. S1B compares the integrated electrodes with a strawberry. As shown in Fig. S1C, the designed flexible electrodes can also be prepared by etching in large quantities.

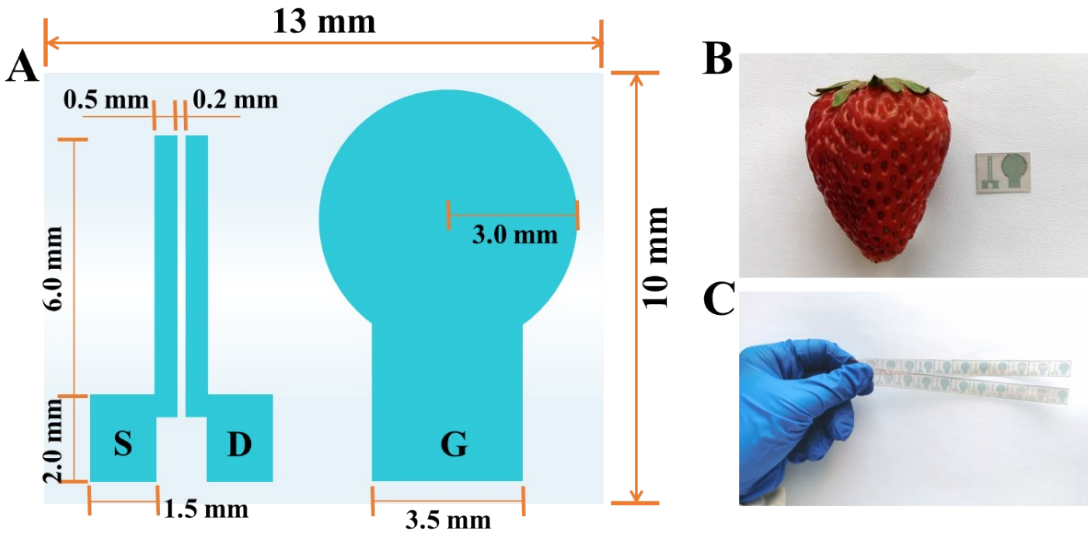

Fig. S1 (A) Schematic diagram of integrated flexible electrodes of OPECT. (B) Comparison of integrated electrodes and a strawberry. (C) Schematic diagram of integrated electrodes etched in large quantities.

2.2 Preparation of gate electrodes.

Preparation of ZnO nanorod arrays (NRs) electrodes. Vertically aligned ZnO NRs were directly grown on flexible ITO-PET electrode by a hydrothermal way. First, the source and drain electrode of the etched and cleaned ITO-PET substrate was attached to with high-temperature sealing film, and the part of gate electrode was then coated with ZnO liquid precursors. Subsequently, $Zn(Ac)_2$ (0.0549 g) were added to ethanol (50 mL) to obtain a ZnO liquid precursors. And then the ZnO liquid precursors was spun onto the ITO-PET electrode surface at 500 rpm, 30s; 3000 rpm, 30s using spin coater. After the ITO-PET electrode was placed in drying oven at 135 ^{o}C for 2 h, they were placed with the conductive surface downward in the growth solution of 40mM methenamine and 40mM zinc nitrate and hydrothermally treated under 95 ^{o}C for 5h. Finally, the ZnO NRs electrodes were prepared by washing with ultrapure water and ethanol and drying in drying oven at 60 ^{o}C for 2 h.

Preparation of $Zn_{1-x}O$ NRs electrodes.[2] The DES was formed at room temperature by combining choline chloride (Meryer, 99%) and ethylene glycol (Sigma–Aldrich, 99.8%) in a 1:2 molar ratio. The ZnO NRs electrode was immersed in DES solution, and the temperature was raised to 80°C and kept for 10 h. Then take the ZnO NRs electrode out of the DES and rinse it repeatedly with ultrapure water, named $Zn_{1-x}O$ NRs.

Preparation of Pd NPs/$Zn_{1-x}O$ NRs electrodes. The $Zn_{1-x}O$ NRs electrodes were fixed on the beaker wall, then $Pd(NO_3)_2$ solution (40 mL) with a concentration of 0.15 mg/mL was added to the beaker. After continuous stirring for 3 h, 7.5 mg NH_3BH_3 was added in the stirred state slowly and continued to stir for 5 h. Finally, the electrodes were removed from the beaker and rinsed three times with ultrapure water to obtain the Pd NPs/$Zn_{1-x}O$ NRs electrodes.

2.3 Preparation of channel.

First, the prepared gate electrode of ITO-PET was sealed with a high temperature resistant sealing film. Then the sealing film above the source and drain electrode was torn off before the channel material was prepared on it. Specifically, a PEDOT:PSS solution containing 5% v/v dimethyl sulfoxide was spin-coated on the top of the channel

with a speed of 2000 rpm to form a layer of thin film. The device was annealed at 130 ^{o}C in nitrogen atmosphere for 10 min and then annealed at 150 ^{o}C for 1 h.

2.4 Fabrication of the OPECT aptasensor.

All aptamer molecules were dissolved in PBS (0.1 M, pH = 7.4). Aptamer probes were immobilized onto the Pd NPs/$Zn_{1-x}O$ NRs gate electrodes via the classic coupling reaction between the amino (-NH_2) groups on aptamer probes and aldehyde (-CHO) groups on glutaraldehyde (GA). Firstly, 10 μL chitosan solution (CHI, 0.1%) with -NH_2 was coated onto the electrodes surface and placed the electrodes under an infrared light to dry. The gate electrodes were further modified with 20 μL glutaraldehyde (GA, 2.5%) by incubating at room temperature for 1 h to combine the -NH_2 on CHI with -CHO on GA, then washed with PBS carefully. Subsequently, aptamer solution (20 μL, 1 μM) with -NH_2 was added to the surface of the gate electrode and incubated at 4 ^{o}C (6 h) to obtain Apt/Pd NPs/$Zn_{1-x}O$ NRs. Then bovine serum protein (BSA, 20 μL, 3%) was further modified on the electrode surface and incubated at room temperature for 30 min to seal unbound -CHO groups of GA. Finally, the electrodes were washed with PBS solution and dried at room temperature.

For the hybridization reaction, aptamer targets (OTA toxin, 20 μL) with different concentrations were dropped on the Apt/Pd/$Zn_{1-x}O$ gate electrodes for 45 min incubation at 37 ^{o}C. Then, the OTA/Apt/Pd NPs/$Zn_{1-x}O$ NRs gate electrodes were obtained by washing carefully three times with PBS solution to remove the unhybridized OTA toxin.

2.5 Electrical measurements

OPECT devices were tested in the electrolyte of PBS solution (0.1M, pH 7.4). For transfer characteristics (I_{DS}-V_G), the channel current I_{DS} was measured as a function of gate voltage V_G under a constant drain voltage V_{DS} = −0.2 V. The channel current I_{DS} as a function of time (I_{DS}-time) was measured under constant gate and drain voltages (V_{DS} = −0.2 V, V_G = 0 V) under illumination.

For the PEC measurements, the PBS solution (0.1M, pH 7.4) was also used as the electrolyte. The photocurrent was measured with a three-electrodes system (ZnO NRs

electrode as the working electrode, a saturated calomel electrode as the reference electrode, and a Pt wire as the counter electrode) at a constant potential of 0 V. The photovoltage, electrochemical impedance spectroscopy (EIS), cyclic voltammograms (CV) and Mott-Schottky were also tested using a three-electrode system (ZnO NRs electrode as the working electrode, a saturated calomel electrode as the reference electrode, and a Pt wire as the counter electrode). The EIS tests were recorded in 0.1 M KCl solution containing $Fe(CN)_6^{3-/4-}$ (5 mM) in a frequency range from 0.1 Hz to 100 kHz; The open circuit potential was used as a DC bias potential, on which amplitude of the AC potential was 5 mV. All the working electrodes ensure the same quality of material in the same working area.

2.6 The detection process of actual sample.

Wine samples, obtained from the local store, were diluted with 1x PBS in a 1:10 ratio without any specific pre-treatment. To prepare spiked wine solution, the proper concentration of OTA in PBS was added to diluted wine. In this way, three different concentrations of OTA toxin standard solutions were spiked into the diluted wine. Finally, the recoveries of three different concentrations of OTA toxin in the spiked wine samples were obtained using the OPECT aptasensor and enzyme-linked immune sorbent assay (ELISA).

3. Results and Discussion

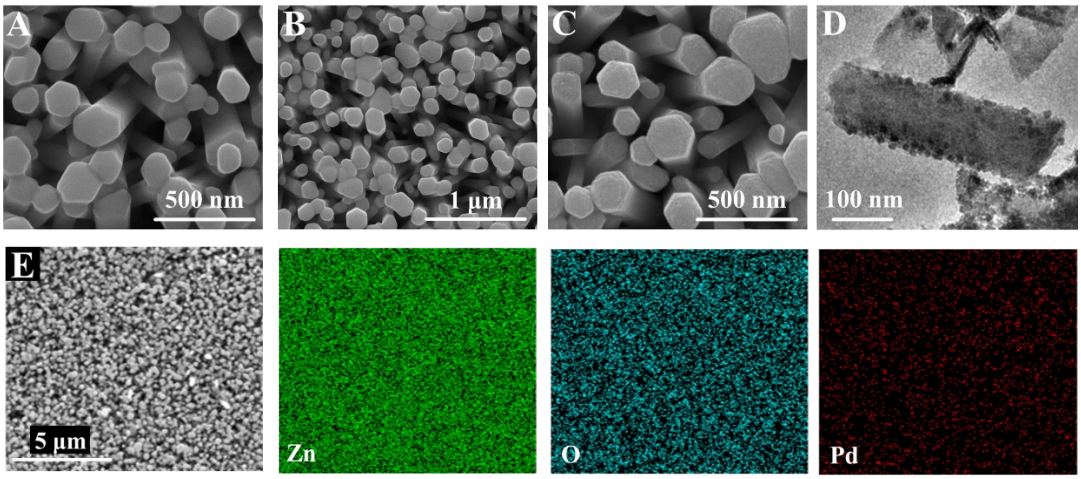

Fig. S2 SEM images of (A) ZnO, (B) $Zn_{1-x}O$ NRs and (C) Pd/$Zn_{1-x}O$. (D) TEM images of Pd/$Zn_{1-x}O$. (E) Element mapping of Pd/$Zn_{1-x}O$.

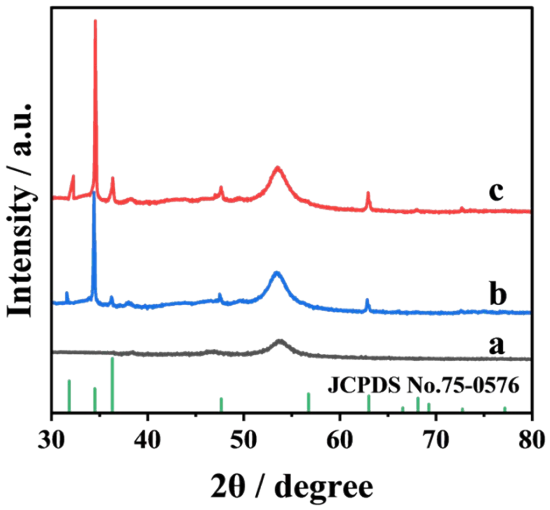

Fig. S3 XRD measurements of (a) ITO-PET, (b) ZnO NRs and (c) Pd NPs/$Zn_{1-x}O$ NRs.

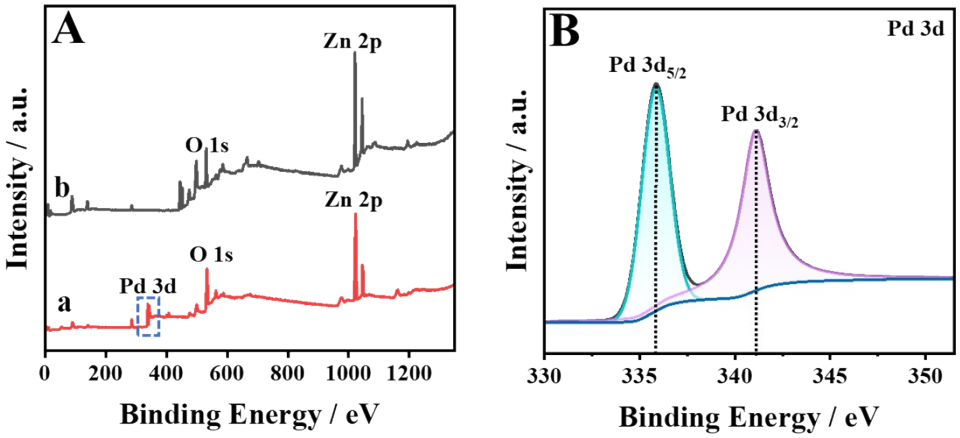

Fig. S4 (A) XPS spectra of Pd NPs/$Zn_{1-x}O$ NRs and (b) $Zn_{1-x}O$ NRs. (B) High-resolution XPS spectra of Pd for Pd NPs/$Zn_{1-x}O$ NRs.

Comparison of Pd 3d, Zn 2p and O 1s X-ray photoelectron spectroscopy (XPS) spectra of Pd NPs/$Zn_{1-x}O$ NRs, with the control sample of ZnO, was performed to explore the electronic structure of Pd NPs/$Zn_{1-x}O$ NRs (Fig. S4A). Fig. S4B displays the Pd 3d XPS spectra of the Pd NPs/$Zn_{1-x}O$ NRs. The Pd 3d spectrum is suit with two peaks, respectively, and the binding energies at 335.8 eV and 341.1 eV correspond to Pd^{2+} $3d_{5/2}$ and Pd^{2+} $3d_{3/2}$.[3, 4]

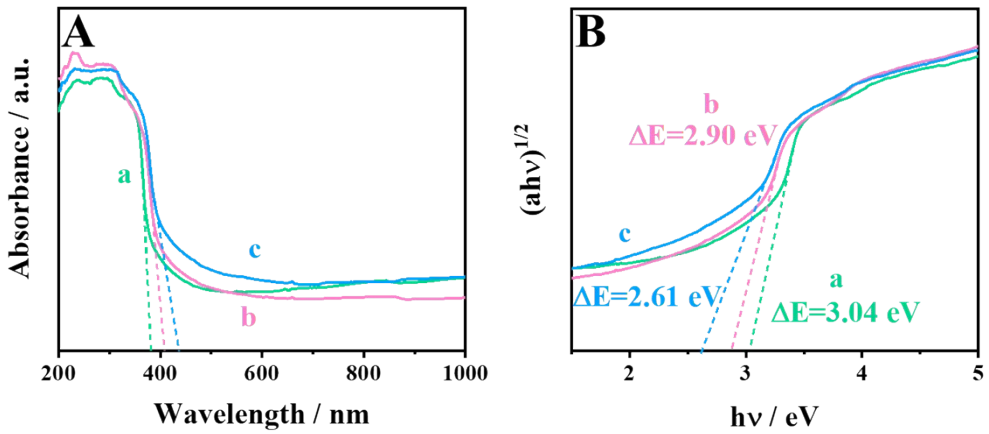

Fig. S5 (A) UV–vis absorption spectra and (B) Plots of $(\alpha h\upsilon)^{1/2}$ versus the energy ($h\upsilon$) for the band gap energy of ZnO NRs(a), $Zn_{1-x}O$ NRs (b) and Pd NPs/$Zn_{1-x}O$ NRs (c).

UV−vis diffuse reflectance spectra (Fig. S5) displayed that compared with ZnO NRs, $Zn_{1-x}O$ NRs showed an enhancement of light absorption, which was red-shifted relatively on account of the presence of Zn vacancies. After loaded Pd NPs, the light absorption of Pd NPs/$Zn_{1-x}O$ NRs was further enhanced which was ulteriorly red-shifted on account of the presence of Schottky junction. Meanwhile, the optical bandgap (Eg) of ZnO NRs, $Zn_{1-x}O$ NRs and Pd NPs/$Zn_{1-x}O$ NRs could be calculated to be 3.04, 2.90 and 2.61 eV, as shown in Fig. S5B.

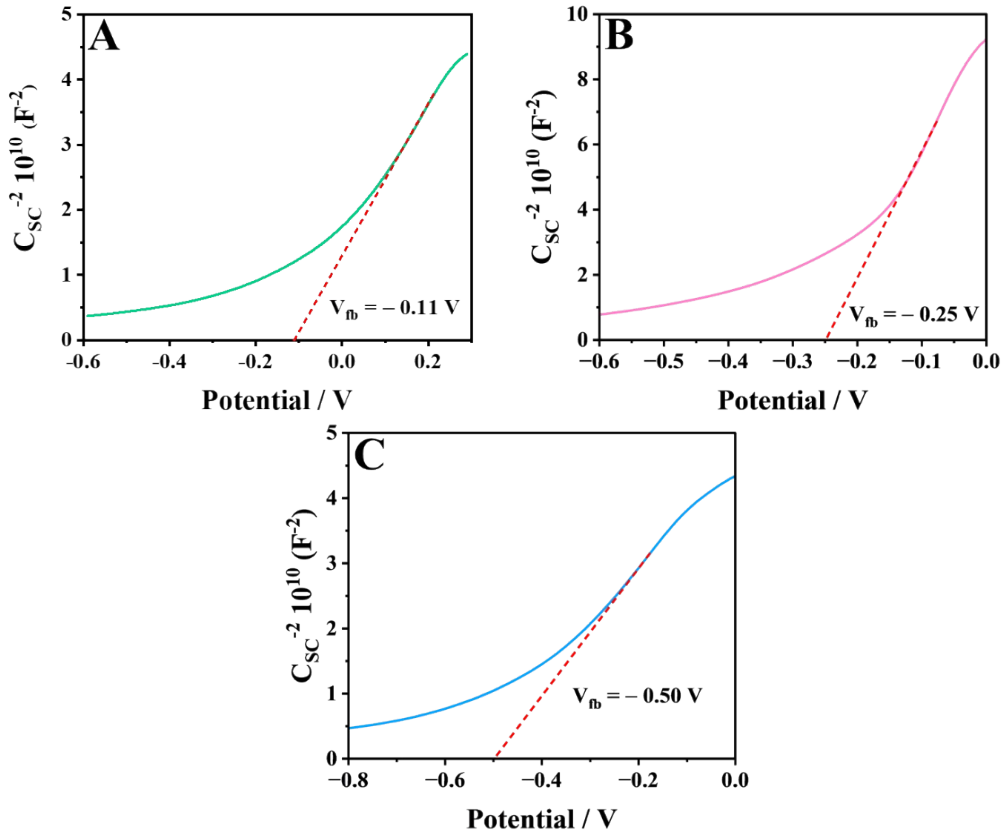

Fig. S6 Mott–Schottky plots of (A) ZnO NRs, (B) $Zn_{1-x}O$ NRs and (C) Pd NPs/$Zn_{1-x}O$ NRs measured in 0.5 M Na_2SO_4 solution at a measuring frequency of 100 Hz.

Electrochemical Mott–Schottky experiments were measured to study the energy band structures of ZnO NRs, $Zn_{1-x}O$ NRs and Pd NPs/$Zn_{1-x}O$ NRs concretely (Fig. S6). The flat band potential (V_{fb}) of the electrodes can be calculated by making the intersection of the extension line of the Mott–Schottky diagram and the horizontal axis.[5] According to Fig. S6, the V_{fb} of ZnO NRs, $Zn_{1-x}O$ NRs and Pd NPs/$Zn_{1-x}O$ NRs were -0.11 V vs. SCE (0.54 V vs. RHE), -0.25 V vs. SCE (0.40 V vs. RHE) and -0.50 V vs. SCE (0.15 V vs. RHE), respectively. Thus, the E_{CB} of ZnO NRs, $Zn_{1-x}O$ NRs and Pd NPs/$Zn_{1-x}O$ NRs are 0.34, 0.20 and -0.05 V, which is 0.2 V more negative than that of the V_{fb}.[6] Based on the formula $E_g = E_{VB} + E_{CB}$, the energy band positions of Zn_1O NRs, $Zn_{1-x}O$ NRs and Pd NPs/$Zn_{1-x}O$ NRs can be schematically drawn in Fig. 1C.

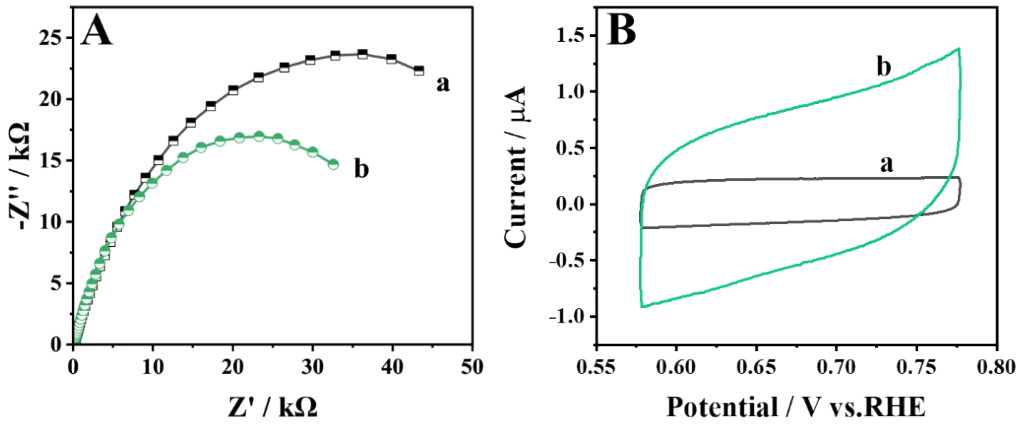

Fig. S7 (A) EIS Nyquist plots of ZnO NRs (a) and Pd NPs/$Zn_{1-x}O$ NRs (b). (B) CV of the ZnO NRs (a) and Pd NPs/$Zn_{1-x}O$ NRs (b) at a scan rate of 50 mV/s.

As evidenced by the electrochemical impedance spectroscopy (EIS) in Fig. S7A, the lower electrochemical impedance of Pd NPs/$Zn_{1-x}O$ NRs was beneficial to the transport of photo-induced electron, compared with ZnO NRs. In addition, Fig. S7B revealed that the increased electrochemical active areas of Pd NPs/$Zn_{1-x}O$ NRs compared with ZnO NRs suggesting the facilitation to electrochemical reaction of synergistic effect between Schottky junction and Zn vacancies.

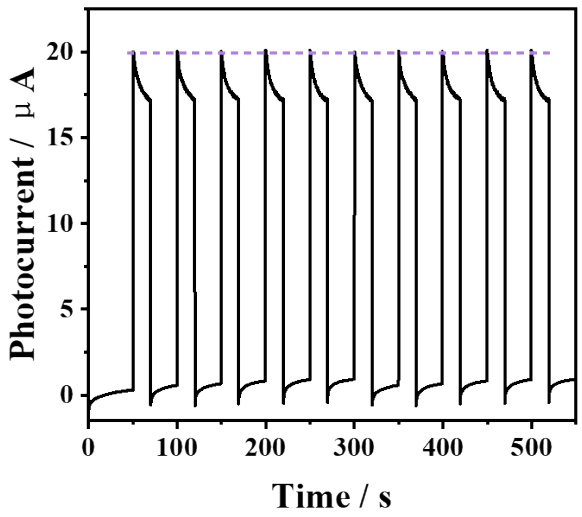

Fig. S8 PEC stability of Pd NPs/$Zn_{1-x}O$ NRs in several repeated light on/off cycles for 1000 s.

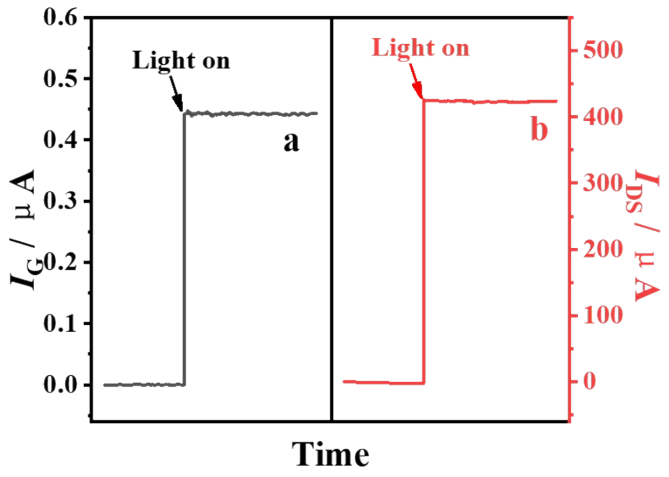

Fig. S9 I_G (a) and I_{DS} (b) of Pd NPs/$Zn_{1-x}O$ NRs gate electrode under illumination.

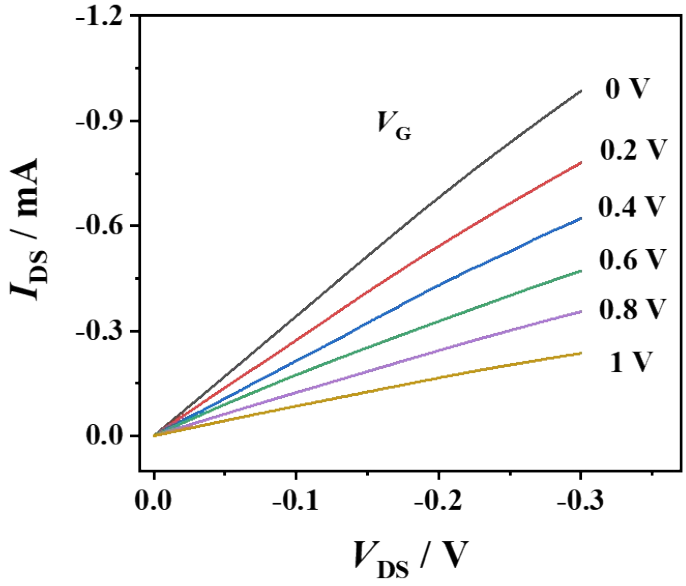

Fig. S10 The output characteristics (I_{DS}-V_{DS}) of the OPECT sensing platform.

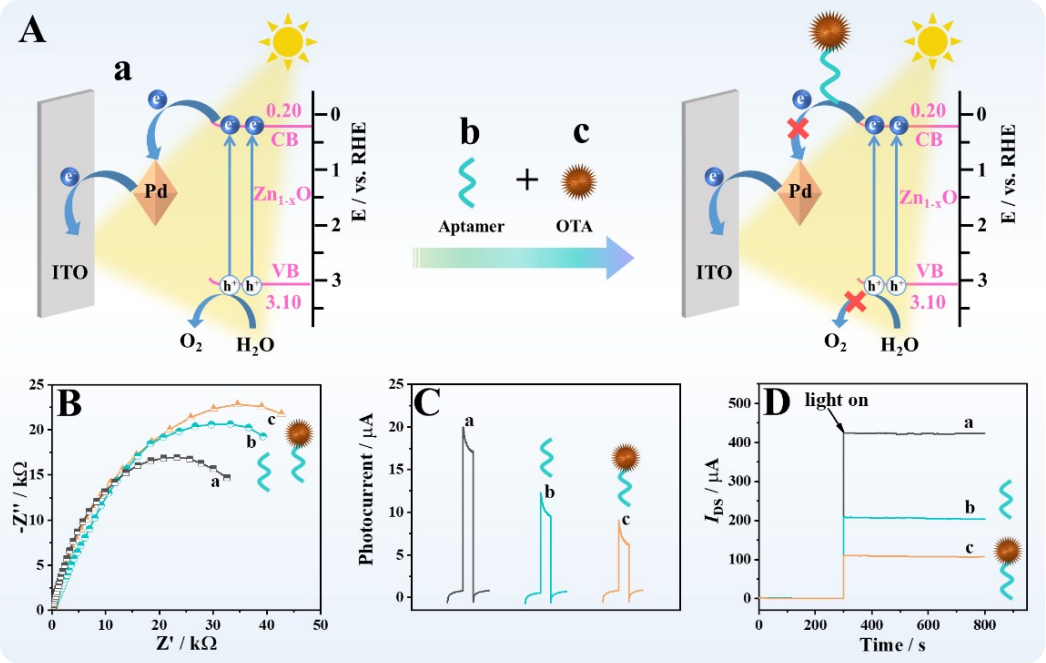

Fig. S11 (A) The schematic illustrating of the integrated OPECT aptasensor. (B) EIS Nyquist plots, (C) Photocurrent in PEC aptasensor and (D) I_{DS} in integrated OPECT aptasensor of Pd NPs/$Zn_{1-x}O$ NRs (a), Apt/Pd NPs/$Zn_{1-x}O$ NRs (b) and OTA/Apt/Pd NPs/$Zn_{1-x}O$ NRs (c).

To research the step-by-step assembly process of this aptasensor, the EIS Nyquist plots, photocurrent and I_{DS} signals with persistent irradiation were investigated as shown in Fig. S11B, C and D, respectively. The initial photocurrent and I_{DS} values of Pd NPs/$Zn_{1-x}O$ NRs separately can be reached the highest values of 17.5 μA (Fig. S11C, curve a) and 423 μA (Fig. S11D, curve a). After further modification of the aptamer, the photocurrent responses decreased from 17.5 μA to 9.7 Ma (Fig. S11C, curve b), corresponded the decreased I_{DS} from 423 μA to 206 μA (Fig. S11D, curve b). This can be interpreted as the inherent steric effects of the aptamer, which hindered the transfer of electron (Fig. S11B, curve b), resulting in a large decrease in photocurrent and ultimately reduced I_{DS} response.[7, 8] Subsequently, analyte (OTA) was incubated on the electrodes so that the aptamer could capture the OTA as much as possible. As a consequence, the photocurrent response drops again to 6.4 μA (Fig. S11C, curve c) and I_{DS} value drops again to 108 μA (Fig. S11D, curve c). This can be attributed to the intrinsic insulation and steric hindrance of OTA (Fig. S11B, curve c), further hindered

the oxidizing reaction between photo-generated holes and H_2O by obstructing the diffusion of photo-generated holes to the interface in contacted with H_2O.[9] Thus, the constructed OPECT aptasensor can be applied to the quantitative analysis and detection of OTA by the changed signal arising from specific binding of aptamer.

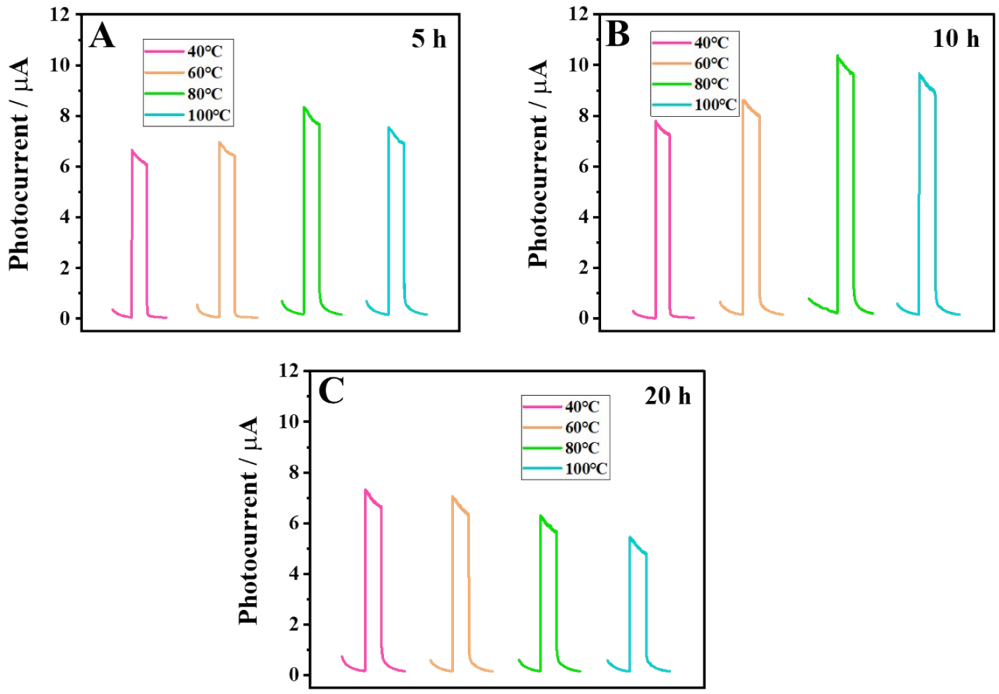

Fig. S12 Photocurrent of DES treated ZnO electrode at different reaction temperatures for different reaction times measured in 0.1 M PBS solution.

The ZnO NRs electrode was directly immersed in a DES solution to leach Zn atoms from ZnO lattices after being heated at different temperatures and for different amounts of time. After being optimized in DES, the $Zn_{1-x}O$ NRs electrodes exhibited the best PEC performance at 80 °C for 10 h.

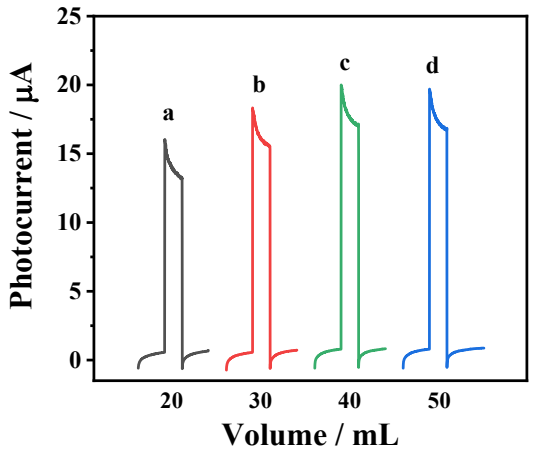

Fig. S13 Effect of different volumes of $Pd(NO_3)_2$ solution on photocurrent of Pd NPs/$Zn_{1-x}O$ NRs electrode.

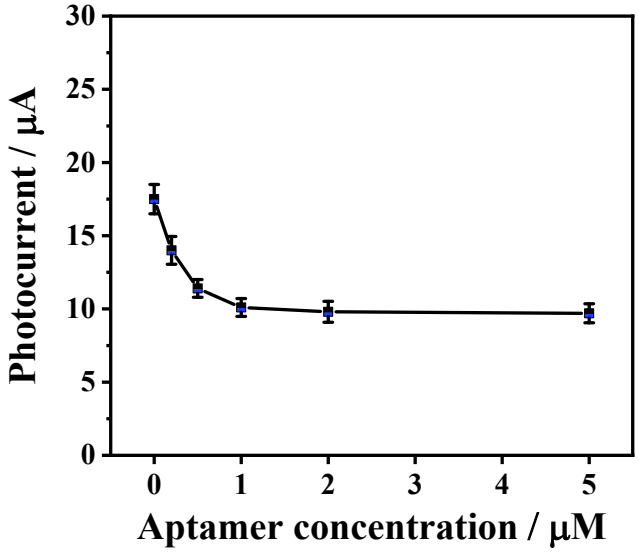

Fig. S14 Effect of aptamer concentration on current of Pd NPs/$Zn_{1-x}O$ NRs electrode.

In addition, the concentration of the aptamer modified onto the gate electrode has an impact on the current for the device. To obtain the best OPECT response, the concentration of the aptamer was optimized. The effects of different concentrations of OTA aptamers on the photocurrent in PEC device are illustrated in Fig. S14. When the concentration of OTA aptamer increased to 1μM, the photocurrent intensity tended to be stable. Therefore, 1 μM was optioned as the optimal concentration to modify on the gate electrode.

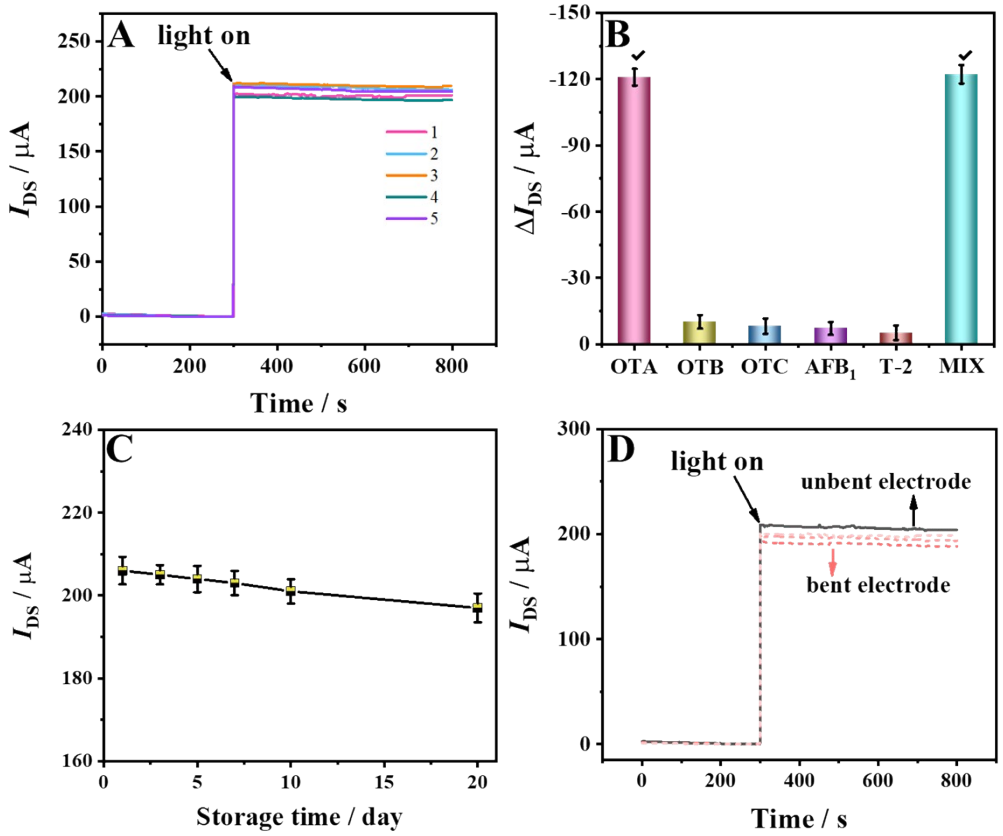

Fig. S15 (A) The reproducibility, (B) selectivity and anti-interference ability, (C) long-term storage stability and (D) pliability of the integrated OPECT aptasensor.

The reproducibility was examined by analyzing five electrodes prepared from the same batch, and the relative standard deviation between them was only 2.6%, indicating the good reproducibility of the OPECT sensing platform (Fig. S15A). The selectivity and anti-interference ability of the sensor was investigated with several interference samples, including 10 ng/L of ochratoxin B (OTB), ochratoxin C (OTC), aflatoxin B1 (AFB1), T-2 toxin (T-2) and their mixture. Fig. S15B shows that only the 1 ng/L of OTA and the mixture could remarkably reduce the I_{DS} despite the concentration of interferents 10-fold higher than that of OTA, demonstrating the considerable selectivity and anti-interference ability of the prepared OPECT aptasensor. Furthermore, after the integrated OPECT aptasensor having been stored at 4 °C for 20 days, the I_{DS} response remained at around 95.6% of the initial signal, manifesting excellent robustness and long-term storage stability (Fig. S15C). In addition, the flexibility of the integrated OPECT aptasensor was tested. As shown in Fig. S15D, after the flexible electrode was

bent in a certain extent, the I_{DS} signal only decreased by 3.2% to 7.3% of the initial I_{DS}, indicating the favorable flexibility of the integrated flexible electrode.

Table S1. Comparison with other detection methods for detecting OTA toxin.

Methods	Liner range (μg/L)	Detection limit (ng/L)	Refs.
Multiplexed self-powered sensor	0.001-20	0.18	[10]
Electrochemiluminescence aptasensor	0.5-4	170	[11]
Electrochemiluminescence biosensing platform	0.00001-0.1	0.0047	[12]
Photoelectrochromic sensor	1-100	330	[13]
Photoelectrochemical sensor	0.000005-10	0.00173	[14]
OPECT aptasensor	0.00002-20	0.00188	This work

Table S2. Determination of T-2 toxin in milk samples using the OPECT aptasensor and ELISA (n = 3).

Samples	Added (μg/L)	Developed assay			ELISA		
		Found (μg/L)	Recovery (%)	RSD (%)	Found (μg/L)	Recovery (%)	RSD (%)
1	0	0	-	-	0	-	-
2	0.1	0.104	104.13	3.73	0.088	87.57	6.30
3	1.0	0.98	98.37	2.48	0.97	96.77	4.18
4	10.0	10.06	100.61	1.01	9.91	99.07	2.03

References

1. J. A. Cruz-Aguado and G. Penner, *Anal. Chem.*, 2008, **80**, 8853-8855.
2. J. Lai, L. Ding, C. Fan, J. Wei, J. Qian and K. Wang, *Chem. Commun.*, 2023, **59**, 75-78.
3. L.-L. Ling, W. Yang, P. Yan, M. Wang and H.-L. Jiang, *Angew. Chem. Int. Ed.*, 2022, **61**, e202116396.
4. L. Li, Z. Li, W. Yang, Y. Huang, G. Huang, Q. Guan, Y. Dong, J. Lu, S.-H. Yu and H.-L. Jiang, *Chem*, 2021, **7**, 686-698.
5. Y. Gong, X. Zhao, H. Zhang, B. Yang, K. Xiao, T. Guo, J. Zhang, H. Shao, Y. Wang and G. Yu, *Appl. Catal., B*, 2018, **233**, 35-45.
6. Y. Zhi, Y. Yi, C. Deng, Q. Zhang, S. Yang and F. Peng, *ChemSusChem*, 2022, **15**, e202200860.
7. Y.-Z. Shen, J. Guan, C. Ma, Y. Shu, Q. Xu and X.-Y. Hu, *Anal. Chem.*, 2022, **94**, 1742-1751.
8. B. Liu, Y. Ge, Y. Lu, Y. Huang, X. Zhang and X. Yuan, *Biosens. Bioelectron.*, 2023, **229**, 115241.
9. L. Ding, Y. Liu, J. Lai, W. Zhu, C. Fan, N. Hao, J. Wei, J. Qian and K. Wang, *Adv. Funct. Mater.*, 2022, **32**, 2202735.
10. J. Wei, Q. Hu, Y. Gao, N. Hao, J. Qian and K. Wang, *Anal. Chem.*, 2021, **93**, 12690-12697.
11. Y. Huang, F. Luo, J. Wang, L. Wang, B. Qiu, C. Lin and Z. Lin, *Anal. Chem.*, 2021, **93**, 17127-17133.
12. X. Zhong, S.-S. Yang, N. Liao, R. Yuan and Y. Zhuo, *Anal. Chem.*, 2021, **93**, 5301-5308.
13. N. Hao, Y. Zuo, Z. Dai, M. Xiong, J. Wei, J. Qian and K. Wang, *Anal. Chem.*, 2021, **93**, 14053-14058.
14. C. Chen, X. Zhou, Z. Wang, J. Han and S. Chen, *Anal. Chim. Acta*, 2022, **1216**, 339943.